Inverted BER Trends for Energy-Detected GRSM-MQAM Massive MIMO Downlink

Oshin Daoud*, Haïfa Farès*, Yahia Medjahdi†, Laurent Clavier†‡, Amor Nafkha*
*IETR - UMR CNRS 6164, CentraleSupélec, avenue de la Boulaie - CS 47601 35576
{oshin.daoud, haifa.fares, amor.nafkha}@centralesupelec.fr
†IMT Nord Europe, Institut Mines-Télécom, Centre for Digital Systems, F-59653 Villeneuve d'Ascq, France
‡IEMN - UMR CNRS 8520, University of Lille, France
{yahia.medjahdi, laurent.clavier}@imt-nord-europe.fr

***Abstract*—This work investigates Generalized Receiver Spatial Modulation (GRSM) in a massive MIMO downlink scenario over millimetre wave channels. While GRSM enhances spectral efficiency (SE) and reduces power consumption, indexing additional bits using the spatial dimension increases the vulnerability to detection errors. These errors primarily stem from threshold-dependent spatial detection. We propose a novel predefined threshold computation method minimizing spatial detection errors, rigorously validated through the Maximum A Posteriori (MAP) criterion. Furthermore, we derive an analytical Average Bit Error Probability (ABEP) expression tailored for energy detection, exploiting inherent constellation energy distributions. The analytical derivation was validated via link-level simulations under two scenarios: (i) perfect spatial detection, and (ii) practical spatial detection. The results show spatial errors dominating overall performance, shifted from theoretical values by practical spatial detection using multiple thresholds for different energy levels in 16QAM. Crucially, an inverted error trend revealed between GRSM-4QAM and GRSM-16QAM, highlighting a trade-off between error resilience, complexity, and energy efficiency.**

***Index Terms*—Generalized Receiver Spatial Modulation, binary activation pattern, mm-wave channel, Receiver Antenna Selection, per-antenna Spatial Detector, Energy Detection.**

I. Introduction

Spatial Modulation (SM) is one of the latest approaches within the Massive MIMO framework. SM is applied to both components of the communication chain: at the transmitter, it is known as Transmitter Spatial Modulation (TSM) [1] and, at the receiver, it is referred to as Receiver Spatial Modulation (RSM) [2]. In both cases, the spatial dimension is exploited to send more bits, which increases the Spectral Efficiency (SE). The spatial bits represent an activation pattern used to activate only one transmit or receive antenna while keeping the others silent, alongside increasing spectral efficiency, it increases the energy efficiency. Unlike TSM, RSM activates all transmit antennas but switches only one receive antenna, thereby preserving the beamforming gain needed to overcome mmWave path loss. A generalized version (GRSM) allows multiple receive antennas to be active [2]–[4].This is achieved via a precoder that directs energy to the active receive antennas while suppressing the others; in the single-user case, it effectively performs beamforming toward the activated antennas. Combinatorial activation patterns are tabulated in look-up tables, where each pattern is used to activate N_a antennas out of N_r total antennas at the receiver. Each pattern contains a fixed number of ones equal to N_a and a fixed number of zeros equal to $N_r - N_a$. The total number of possible combinations is given by the binomial coefficient: $\binom{N_r}{N_a}$. Alternatively, in [5], the random N_a-bit activation pattern is used directly without look-up tables. The spatial symbol of N_a bits is used, allowing 2^{N_a} binary combinations. This means the number of ones and zeros will vary depending on the binary combination and their positions, which aligns with the Variable active Antenna Spatial Modulation (VASM) proposed in [6]. In [5], the all-zeros binary activation pattern is excluded to prevent deactivation of all N_a receive antennas. In contrast, [6] handles this case by activating a default antenna when the all-zeros pattern occurs.

In mm-wave communication, high spatial correlation, due to limited scattering and dominant line-of-sight (LoS) propagation, makes it difficult to distinguish between receiving and non-receiving antennas using precoding. This necessitates antenna decorrelation for improved performance. In indoor environments, the spacing between the transmitter antennas d_t and receiver antennas d_r can be chosen to ensure that the paths of the channel matrix are approximately orthogonal, thereby minimizing the symbol error rate (SER), as demonstrated in [3]. In outdoor environments, achieving similar decorrelation may require larger antenna arrays or increased spacing, particularly when the transmitter-receiver distance is large [5].

In [7], an efficient Transmitter Antennas Combinations (TAC) selection method is performed without using instantaneous CSI, based on minimizing the transmitter spatial correlation in highly correlated mmwave channel. The approach in [5], used the Receiver Antenna Selection (RAS) to optimize the Receiver Antenna Combination (RAC) by selecting the least correlated N_a receiver antennas. This reduces the channel matrix $\mathbf{H} \in \mathbb{C}^{N_r \times N_t}$, into a sub-matrix $\mathbf{H}_a \in \mathbb{C}^{N_a \times N_t}$.

Detection in all SM-based schemes typically involves two stages: one for detecting the spatial symbols and another for detecting the modulated symbols. A common approach found in the literature relies on decoupled detection, where the spatial and modulated symbols are detected separately using the maximum likelihood (ML) criterion [2], [4]. The second approach exploits a more complex but optimal detector that detects both spatial and modulated symbols jointly as in [1], [3],

979-8-3503-9281-4/25/$31.00 ©2025 IEEE

[6], [7]. In [5], a decoupled detection strategy was exploited, assuming an ML detector for the modulated symbols detector and a per-antenna amplitude detector to detect the spatial bits in one spatial symbol. The amplitude detector determines the spatial bit by comparing the amplitude of the received signal at each receive antenna with an instantaneous threshold. Two different thresholding approaches are proposed. The exact threshold comes with significant computational complexity, as it requires instantaneous calculation based on the current received signal amplitude. Moreover, its derivation assumes a uniform probability distribution of spatial bits, an idealized assumption that may not be valid in practical implementations, especially considering that the all-zeros binary pattern has been excluded. The alternative threshold proposed in [5] is an approximation designed for moderate to high SNR regimes. However, it does not account for low SNR conditions and requires an additional pilot transmission from the transmitter to the receiver within the Time Division Duplexing (TDD) protocol for its estimation.

In this paper, we apply the GRSM with binary activation patterns to a single-user downlink massive MIMO system operating at 28 GHz. We formulate the detection of the received signal as an energy sensing problem seeking a simpler mathematical processing than the one in the amplitude detection, where the goal is to detect the N_a spatial bits using a per-antenna energy detector. To avoid the complexity of the instantaneous exact threshold and the need for additional pilot symbols required by the approximate threshold, we propose an optimal threshold that minimizes the spatial bit error probability. This threshold is predefined, as it is derived from the energy levels of the MQAM constellation rather than the instantaneous received signal energy, and therefore, its merit is threefold: it does not require additional pilot symbols for calculation, it is less complex since it is not instantaneously calculated, and it remains consistent across all SNR ranges. Besides, it is validated using the MAP decision rule while accounting for the unequal probabilities of binary values 1 and 0, which arise due to the exclusion of the all-zeros combination from the spatial constellation. Furthermore, we derive a generic Average Bit Error Probability (ABEP) by considering both spatial and modulation symbols, capturing the influence of MQAM constellation energy levels and their probabilities. We provide an integrated performance evaluation, which includes the total ABEP and analyze the results separately for the spatial and the modulation bits. Our analytical results are thoroughly validated through Monte Carlo link-level simulations, which evaluate the total Bit Error Rate (BER) along with its spatial and modulation error components. In these simulations, two different spatial detection approaches are used to select the predefined threshold from the lookup tables in the 16QAM case, where the threshold varies over three energy levels in 16QAM constellation. The first is a perfect approach used for validation purposes, assuming that the receiver has perfect knowledge of the transmitted symbol's energy level. It serves as a lower bound on the error performance. The second is a practical approach based on exhaustive search, where the receiver estimates the energy level, showing only minor performance degradation compared to the ideal case. Counterintuitively, under fixed spectral efficiency, higher-order GRSM-MQAM schemes demonstrate improved error performance. This reveals an important trade-off: although higher-order MQAM increases energy consumption, it can lead to significantly better error performance.

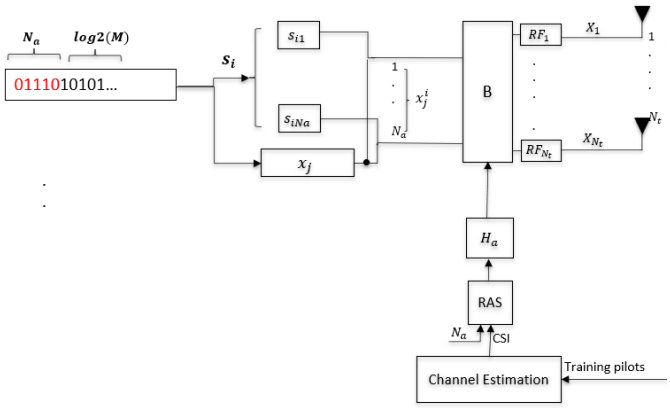

Fig. 1. The fully digital Massive MIMO transmitter structur with GRSM.

II. The System Model

A. The Transmitter

The transmitter is a fully digital Base Transceiver Station (BTS) equipped with N_t antennas as depicted in Fig. 1. The random binary input stream is partitioned into two streams: the first N_a bits represent the spatial symbol, and $\log_2(M)$ bits are representing the MQAM modualted symbol. Since the activation patterns are determined by the 2^{N_a} possible combinations of the spatial symbol, one of these combinations corresponds to the all-zero pattern, which results in deactivating all receiver antennas prohibiting the receiver from catching any meaningful signals. To prevent this undesired scenario, the all-zero combination is excluded from the set of valid spatial symbols. This exclusion slightly affects the uniformity of the ones and zeros distribution, introducing a bias in the probabilities of 1 and 0 in the activation patterns. The modulated symbol used in MQAM modulation belongs to the constellation $\mathcal{C} = \{x_j \mid j \in \{1, \ldots, M\}\}$, and the spatial symbol is defined as $\mathbf{s}_i \in \{0,1\}^{N_a \times 1} \subset \mathbb{C}^{N_a \times 1}$, where $i \in \{1, \ldots, 2^{N_a} - 1\}$. Thus, the super symbol is defined as: $x_{i,j} = \mathbf{s}_i \; x_j, \in \mathbb{C}^{N_a \times 1}$.
The spectral efficiency is calculated as $\text{SE} = N_a + \log_2(M)$ bits/sec/Hz. As depicted in Fig. 1, for the Time Division Duplexing (TDD) downlink, the transmitter estimates the channel using training pilots sent by the receiver, leveraging channel reciprocity. Assuming that the BTS is perfectly estimating the Channel State Information (CSI), a receiver antenna selection algorithm (RAS) is implemented to select the least N_a correlated receiver antennas by solving the following optimization problem $\min_{\mathbf{H}_a \subseteq \mathbf{H}} \text{Tr}\left\{\left(\mathbf{H}_a \mathbf{H}_a^H\right)^{-1}\right\}$, where $\text{Tr}\{\cdot\}$ denotes the trace function. The N_a bits in each spatial symbol are

mapped to the N_a selected receive antennas using the Zero-Forcing (ZF) precoder $\mathbf{B} = \mathbf{H}_a^H \left(\mathbf{H}_a \mathbf{H}_a^H\right)^{-1} \in \mathbb{C}^{N_t \times N_a}$. The transmitted super vector is $X_{i,j} = \sqrt{\alpha P}\mathbf{B}x_{i,j} \in \mathbb{C}^{N_t \times 1}$, where P represents the average transmit power, and the power normalization factor is given by $\alpha = \frac{1}{\text{trace}\left((\mathbf{H}_a \mathbf{H}_a^H)^{-1}\right)}$. This power normalization factor is always maximized, since we aim to minimize the term $\text{Tr}\left(\left(\mathbf{H}_a \mathbf{H}_a^H\right)^{-1}\right)$ in the receiver antenna selection algorithm. In this work, the average value $\alpha_{\text{aver}} = \mathbb{E}_{H_a}[\alpha]$ is used to avoid the fluctuation of instantaneous values.

B. The mmWave Channel Model

The channel follows an extended Saleh-Valenzuela framework to capture 28 GHz mmWave propagation as a narrowband clustered channel with Line-of-Sight (LOS) and Non-Line-of-Sight (NLOS) components. The discrete-time channel $H \in \mathbb{C}^{N_r \times N_t}$ is given by [8]:

$$H = \beta \sum_{i=1}^{N_c} \sum_{\ell=1}^{N_l} g_{i\ell} \Lambda_r(\phi_{i\ell}^r, \theta_{i\ell}^r) \Lambda_t(\phi_{i\ell}^t, \theta_{i\ell}^t) \\ a_r(\phi_{i\ell}^r, \theta_{i\ell}^r) a_t(\phi_{i\ell}^t, \theta_{i\ell}^t)^\dagger, \tag{1}$$

where $\beta = \sqrt{N_t N_r / (N_c N_l)}$ normalizes the channel, N_c and N_l are the numbers of clusters and rays per cluster, and $g_{i\ell}$ is the complex gain of the ℓ-th ray in the i-th cluster. The angles $\phi_{i\ell}^r(\theta_{i\ell}^r)$ and $\phi_{i\ell}^t(\theta_{i\ell}^t)$ denote the azimuth (elevation) angles of arrival and departure, while $\Lambda_r(\cdot)$ and $\Lambda_t(\cdot)$ are the corresponding antenna element gains. The vectors $a_r(\phi_{i\ell}^r, \theta_{i\ell}^r)$ and $a_t(\phi_{i\ell}^t, \theta_{i\ell}^t)$ represent the normalized receive and transmit array response vectors at these angles, where $(\,)^\dagger$ denotes the Hermitian operator. Both are given for a Uniform Linear Array (ULA) over the y-axis of N elements: $\mathbf{a}_{\text{ULA}_y}(\phi) = \frac{1}{\sqrt{N}} \begin{bmatrix} 1 & \dots & e^{j(N-1)kd\sin(\phi)} \end{bmatrix}^T$, where $k = \frac{2\pi}{\lambda}$, d is the inter-element spacing, and λ is the wavelength.

C. The Receiver

The received signal at N_a receiver branches is given by:

$$\mathbf{y} = \sqrt{\alpha P}\mathbf{H}_a \mathbf{B} s_i x_j + \mathbf{n}, \tag{2}$$

where $\mathbf{y} \in \mathbb{C}^{N_a \times 1}$ and $\mathbf{n} \in \mathbb{C}^{N_a \times 1}$ is the additive white Gaussian noise (AWGN) at the receiver side, modeled as $\mathbf{n} \sim \mathcal{CN}(0, \sigma^2 \mathbf{I}_{N_a})$ where σ^2 represents the noise variance. The received signal at the k-th receiver antenna is given by:

$$y_k = \sqrt{\alpha}\ s_{ik} x_j + n_k, \tag{3}$$

where s_{ik} is either 1 or 0 and $P = 1$. The Energy Detector (ED),shown in Fig. 2, mainly measures the received energy at the k-th branch and the 1-bit ADC compares it to a predefined threshold γ, according to the rule: $\hat{s}_{ik} = 0$ if $z_k < \gamma$, and $\hat{s}_{ik} = 1$ if $z_k \geq \gamma$, where z_k is a random variable depicting the received energy. The wrongly detected $\hat{s}_{ik}$ corresponds to two different types of errors:

- The probability of estimating 0 while 1 is actually mapped (i.e., a missed detection) is given by:

$$P_{md} = \Pr(z_{s_{ik}=1} < \gamma). \tag{4}$$

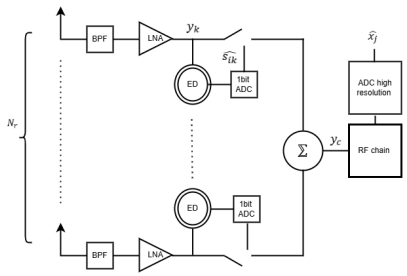

Fig. 2. User Terminal structure.

- The probability of estimating 1 while 0 is actually mapped (i.e., a false alarm) is given by:

$$P_{fa} = \Pr(z_{s_{ik}=0} \geq \gamma). \tag{5}$$

The rest part of the receiver is mainly used to combine the N_a received branches, and then a classical Maximum Likelihood (ML) detector is used to detect the modulated symbols. The detected symbol $\hat{x}_j$ is obtained by applying the maximum likelihood (ML) rule over the MQAM constellation $\mathcal{C}$:

$$\hat{x}_j = \arg\min_{x_j \in \mathcal{C}} |y_c - x_j|^2,$$

where

$$y_c = \sum_{k=1}^{N_a} \left(\sqrt{\alpha}\, x_j\, s_{ik}\, \hat{s}_{ik} + n_k\, \hat{s}_{ik}\right).$$

It is worth mentioning that the combined signal y_c is affected by the performance of the spatial detector due to the presence of switches that are controlled by $\hat{s}_{ik}$. The Table I explains this effect.

III. The Analytical ABEP Derivation

This section derives a general ABEP formula for MQAM constellations by modeling the presence of received signal energy as an energy sensing problem. This is justified by the use of a Zero-Forcing (ZF) precoder, which nulls channel effects and renders the system equivalent to an AWGN channel as shown in (3). As a result, the received energy follows a Chi-Square distribution [9]. The section further analyzes received energy, introduces and validates the proposed detection threshold, defines error probabilities, and presents the generic ABEP expression for GRSM-MQAM systems.

A. The proposed received signal energy model

Starting from (3), when $s_{ik} = 0$, the k_{th} received signal is $y_k = n_k$. It follows a circularly symmetric complex Gaussian (CSCG) distribution: $y_k \sim \mathcal{CN}(0, \sigma^2)$. Decomposing into real and imaginary parts, this leads to : $y_{kR}, y_{kI} \sim \mathcal{N}(0, \sigma^2/2)$. Starting from the existence of two independent and identically distributed (i.i.d.) zero mean normal variables y_{kR} and y_{kI}, the random variable: $z = \frac{|y_k|^2}{\sigma^2/2} \sim \chi_k^2$ follows a central chi-squared distribution with a degree of freedom $k = 2$. The probability density function (PDF) of z is given by [10]:

$$f_0(z) = \frac{1}{2} \exp\left(-\frac{z}{2}\right), \quad z \geq 0 \tag{6}$$

TABLE I
SWITCH OPERATION BASED ON ESTIMATED SPATIAL BIT $\hat{s}_{ik}$

s_{ik}	$\hat{s}_{ik}$	**Switch Status**	**Signal Processing**	**Detection State**
1	1	Closed	y_k passes to the combiner	Correct Detection
1	0	Open	y_k is discarded	Missed Detection (MD)
0	1	Closed	y_k passes to the combiner (only noise passes)	False Alarm (FA)
0	0	Open	y_k is discarded (noise is also discarded)	Correct Detection

For a central chi-squared distributed variable with k degrees of freedom, the complementary cumulative distribution function (CCDF) is:

$$\overline{F_0(z)} = \int_z^{\infty} \frac{1}{2} \exp\left(-\frac{t}{2}\right) dt. \tag{7}$$

Likewise, when $s_{ik} = 1$, the k_{th} received signal becomes $y_k = \sqrt{\alpha}\ x_j + n_k$. Thus, the received signal follows: $y_k \sim \mathcal{CN}(\sqrt{\alpha}\ x_j, \sigma^2)$. Decomposing into real and imaginary parts, both parts are described as: $y_{kR} \sim \mathcal{N}\left(\mathrm{Re}(\sqrt{\alpha}\, x_j), \frac{\sigma^2}{2}\right)$, $y_{kI} \sim \mathcal{N}\left(\mathrm{Im}(\sqrt{\alpha}\, x_j), \frac{\sigma^2}{2}\right)$. Starting from the existence of two independent and identically distributed (i.i.d) nonzero mean normal variables y_{kR} and y_{kI}, random variable: $z = \frac{|y_k|^2}{\sigma^2/2} \sim \chi_k^2(\lambda)$ follows a non-central chi-squared distribution with a degree of freedom $K = 2$ and non-centrality parameter λ. The probability density function (PDF) of z is given by [10] :

$$f_1(z) = \frac{1}{2} \exp\left(-\frac{z+\lambda}{2}\right) I_0\left(\sqrt{z\lambda}\right), \quad z \geq 0 \tag{8}$$

where λ is the non-centrality parameter and $I_0(\cdot)$ is the modified Bessel function of the first kind of order zero. The cumulative density function (CDF) is given by:

$$F_1(z) = \int_0^z \frac{1}{2} \exp\left(-\frac{t+\lambda}{2}\right) I_0\left(\sqrt{t\lambda}\right) dt. \tag{9}$$

To calculate the non-centrality parameter, considering the two normally distributed nonzero mean variables y_{kR} and y_{kI}, we use the equation from [9]: $\lambda = \frac{\mu_1^2}{\sigma_1^2} + \frac{\mu_2^2}{\sigma_2^2}$, where: $\mu_1 = \sqrt{\alpha}\,\mathrm{Re}(x_j)$, $\mu_2 = \sqrt{\alpha}\,\mathrm{Im}(x_j)$, and the standard deviations are given by: $\sigma_1 = \frac{\sigma}{\sqrt{2}}$, $\sigma_2 = \frac{\sigma}{\sqrt{2}}$. Thus, the final non-centrality value is given by:

$$\lambda = \frac{2\alpha}{\sigma^2}\ |x_j|^2. \tag{10}$$

From (10), it is evident that the non-centrality parameter depends on the energy of the modulated symbol. This relationship reveals the internal energy distribution within the non-uniform MQAM constellations. When $M > 4$, the constellation exhibits varying energy levels; for instance, 16QAM modulation scheme contains three distinct energy levels as depicted in Fig. 3. Consequently, three different non-centrality parameters must be defined.

B. The Spatial Error probability P_{es}

Based on the previous description by using the central and non-central chi-square distributions, recalling (7), (5) and (9),(4), the probability of false alarm and the probability of missed detection can be expressed, respectively, as follows:

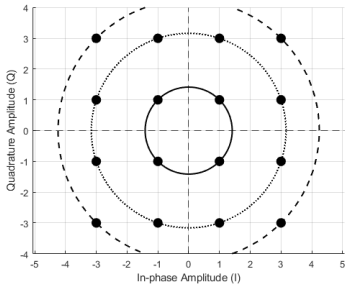

Fig. 3. The energy levels inside the 16QAM constellation: $E_1 = 2$, $E_2 = 10$, $E_3 = 18$; $P_1 = 0.25$, $P_2 = 0.5$, $P_3 = 0.25$; solid, dotted, dashed, respectively.

$$P_{fa} = \int_{\gamma}^{\infty} \frac{1}{2} \exp\left(-\frac{z}{2}\right) dz = e^{-\gamma/2}, \tag{11}$$

$$\begin{aligned} P_{md} &= \int_0^{\gamma} \frac{1}{2} \exp\left(-\frac{z+\lambda}{2}\right) I_0\left(\sqrt{z\lambda}\right) dz \\ &= 1 - Q_1(\sqrt{\lambda}, \sqrt{\gamma}), \end{aligned} \tag{12}$$

where $Q_1(a, b)$ denotes the first-order Marcum Q-function. According to Binary Hypothesis Theory, the overall probability of error P_{es} is

$$P_{es} = \Pr(\mathcal{H}_1) P_{md} + \Pr(\mathcal{H}_0) P_{fa}, \tag{13}$$

where $\mathcal{H}_1$ and $\mathcal{H}_0$ denote the hypotheses of spatial bits 1 and 0, respectively. Since the spatial component increases the system's vulnerability to errors, particularly in threshold-based spatial detectors, we propose an exact threshold that minimizes the spatial error probability defined in (13).This corresponds to finding the zeros of the first derivative of P_{es} with respect to the threshold γ:

$$\frac{dP_{es}}{d\gamma} = 0. \tag{14}$$

Furthermore, this threshold can be selected in advance since the non-centrality parameters can be calculated based on known energy levels of the considered MQAM constellation. Thus, no need to calculate it at each realization. However, this threshold is validated using the Maximum a Posteriori (MAP) principle. As suggested in [11], since the spatial bit probabilities are unbalanced when the all-zero case is excluded, especially for small N_a. The MAP rule, based on Binary Hypothesis Testing, compares the received energy described as z follows $f_1(z|\mathcal{H}_1)$ in (6) and $f_0(z|\mathcal{H}_0)$ in (8).

The MAP decision rule accounts for unequal priors $P(\mathcal{H}_1)$ and $P(\mathcal{H}_0)$ as described in [11].

$$D^{\text{MAP}}(z) = \begin{cases} 1, & \text{if } f_1(z|\mathcal{H}_1)P(\mathcal{H}_1) \geq f_0(z|\mathcal{H}_0)P(\mathcal{H}_0) \\ 0, & \text{if } f_1(z|\mathcal{H}_1)P(\mathcal{H}_1) < f_0(z|\mathcal{H}_0)P(\mathcal{H}_0). \end{cases} \quad (15)$$

The threshold tables are directly used in the analytical ABEP derivation because they inherently account for all energy levels by weighting each level according to its probability, thus, no additional information is required, as will be explained in III-D. However, for ABEP validation via link-level simulation, the application of the detection principle here is not straightforward, particularly for high-order modulation, *i.e.*, $M > 4$. For instance, while the threshold application for 4QAM is direct since a unique predefined threshold is stored for the unique energy level for transmitted symbols, the complexity arises with 16QAM, where three distinct energy levels necessitate selecting the correct threshold from three possibilities. To address this, two methods are employed:

- **Perfect Method:** Assumes ideal receiver knowledge of the transmitted symbol's energy level, providing a theoretical lower bound on error performance. This assumption is used to validate the derived ABEP curves.
- **Practical ML-Based Method:** The receiver does not know the energy level in advance but instead estimates the most likely energy level using a Maximum Likelihood (ML)-based approach. This method reflects a more realistic scenario and provides a practical benchmark for system performance.

This leads to the following minimization:

$$\hat{E} = \underset{E_e \in \xi_{16QAM}}{\operatorname{argmin}} \; |\bar{E} - \alpha E_e|$$

considering the 16QAM energy levels $\xi_{16QAM} = \{E_1, E_2, E_3\}$, where the average received energy is given: $\bar{E} = \frac{1}{w}\sum_{i=1}^{N_a} |y_i|^2$ letting w the average number of ones in the spatial constellation for a given N_a; in otherword, the average number of modulation symbol copies are received. For illustration, we count $w = 2.1333$ when $N_a = 4$.

C. The modulated symbols error probability P_{em}

The error probability of the modulated symbol, denoted as P_{em}, is related to both the classical Bit Error Probability (BEP) for MQAM constellations and the spatial error probability. This dependency arises from the fact that the performance of the spatial detector directly affects the overall signal, as discussed earlier and summarized in Table 1. Considering all sources of error, the expression of the error probability of the modulated symbol follows:

$$P_{em} = \sum_{i=1}^{2^{N_a}-1} \sum_{n=0}^{2^{N_a}-1} \text{BEP}_{x_j \in \mathcal{C}_M}(\text{SNR}_c) \Pr(\hat{s}_n|s_i) \Pr(s_i). \quad (16)$$

$\text{BEP}_{x_j \in \mathcal{C}_M}$ is the bit error probability function of MQAM, and the effective SNR at the combiner is given by:

$$\text{SNR}_c = \left(\frac{(b^{11})^2}{b^{11} + b^{01}}\right) \frac{\alpha E_s}{\sigma^2},$$

where E_s is the average constellation energy. The term $\frac{(b^{11})^2}{b^{11}+b^{01}}$ captures the influence of spatial detection accuracy on the effective SNR perceived by the modulated symbol detector. Here, b^{11} denotes the number of spatial bits correctly detected as 1, while b^{01} corresponds to the number of false alarms, *i.e,* bits incorrectly detected as 1. This metric rewards accurate spatial detection, as the numerator grows quadratically with b^{11} , and it penalizes false alarms through the presence of b^{01} in the denominator. For example, if the transmitted spatial index is $\mathbf{s}_i = 1110$ and the detected index is $\hat{\mathbf{s}}_i = 1101$, then $b^{11} = 2$ and $b^{01} = 1$. In this case, the ratio becomes greater than 1, which amplifies the effective SNR. However, if the detection yields $\hat{\mathbf{s}}_i = 0000$, we assume only receiver noise contributes, and the Bit Error Probability (BEP) is approximated as 0.5, corresponding to random guessing. The conditional spatial detection error probability when $\hat{s}_i$ is the detected spatial symbol, given that the spatial symbol was s_i: $\Pr(\hat{s}_i|s_i) = P_{md}^{b^{10}}(1 - P_{md})^{b^{11}} P_{fa}^{b^{01}}(1 - P_{fa})^{b^{00}}$ and $\Pr(s_i) = \frac{1}{2^{N_a}-1}$.

D. The generic ABEP derivation

In our work, the Chi-square distribution is employed to model the received energy, capturing the inherent variation in energy levels across an MQAM constellation through the non-centrality parameter. The multiple non-centrality parameters lead to distinct spatial and modulation symbol error probabilities, each associated with a specific probability of occurrence. This is because the energy levels in an MQAM constellation occur with different probabilities. These insights lead to a more general expression for the Average Bit Error Probability (ABEP) in GRSM-MQAM systems, one that is specifically tailored to the non-uniform energy distribution inherent in MQAM constellations. The formula is depicted in (17), where e in E_e index the discrete energy levels in the considered MQAM constellation, and P_e denotes the probability of a transmitted symbol having energy e.

IV. Implementation and Results

A. mmwave channel parameters

A Uniform Linear Array (ULA) is used at the receiver and transmitter with $N_r = 8$, $N_t = 32$. Assuming: $N_c = 8$, $N_l = 10$. The clusters azimuth (elevation) angles of arrival/departure, respectively, $\phi_i^r(\theta_i^r)$ and $\phi_i^t(\theta_i^t)$ have a uniform distribution inside the following ranges: Transmitter Beamwidth = 50° in azimuth, 180° in elevation, Receiver Beamwidth is omnidirectional in the azimuth plane, receiving from 0° to 180° in the elevation plane. The average power for the i-th cluster: $g_i \sim \text{i.i.d.}\, \mathcal{CN}\left(0, \sigma_{g,i}^2\right)$. Regarding the rays: azimuth (elevation) angles of arrival and departure, respectively, $\phi_l^r(\theta_l^r)$ and $\phi_l^t(\theta_l^t)$ have a Laplacian distribution.

B. Threshold validation and error performance evaluation:

For a fixed spectral efficiency of SE = 8 bits/sec/Hz, the parameters N_a and M are chosen accordingly: $N_a = 6$ for 4QAM and $N_a = 4$ for 16QAM. To apply the MAP rule, the prior probabilities $P(\mathcal{H}_0)$ and $P(\mathcal{H}_1)$ are computed for each

$$\text{ABEP}_{\text{GRSM-MQAM}} = \frac{\log_2(2^{N_a}-1)\sum_e P_{es,e}P_e + (\log_2 M)\sum_e P_{em,e}P_e}{\log_2(2^{N_a}-1)+\log_2 M} \tag{17}$$

configuration after excluding the all-zero case. For $N_a = 6$, the probabilities are nearly equal, allowing the MAP rule to simplify to the ML rule with $P(\mathcal{H}_0) = P(\mathcal{H}_1) = 0.5$. In contrast, with $N_a = 4$, the prior probabilities differ: $P(\mathcal{H}_0) = 0.4667$ and $P(\mathcal{H}_1) = 0.5333$. The noise variance $\sigma^2 = \frac{E_s}{\text{SNR}_b}$, where $\text{SNR}_b = \frac{\text{SNR}}{\log_2(M)}$.

Fig. 4 shows the resulting threshold values for both cases. In 16QAM, due to its non-uniform constellation, the threshold varies across three levels depending on changes in the non-centrality parameter at each noise level. Notably, the threshold that minimizes spatial detection error matches the exact MAP/ML threshold. Finally, although the energy level $E = 2$ appears in both constellations, it results in different non-centrality parameters and detection thresholds.

Fig. 5 illustrates that the spatial component dominates the overall error performance for both modulation schemes. This behavior is attributed to the fact that the Average Bit Error Probability (ABEP) depends on both M and N_a, varying logarithmically with M, but almost linearly with N_a, thus highlighting the dominant role of the number of spatial streams. Contrary to classical expectations where 4QAM typically outperforms 16QAM, our results show that GRSM-4QAM yields worse ABEP/BER than GRSM-16QAM at low to moderate SNRs. This inversion is due to the added spatial bits N_a inherent in receiver spatial modulation. For a fixed spectral efficiency of 8 bits/sec/Hz, GRSM-4QAM requires more spatial bits, leading to a denser spatial constellation and increased spatial detection errors. Additionally, GRSM-4QAM suffers from an imbalance between spatial and modulation streams, further degrading performance. In contrast, GRSM-16QAM offers a more balanced configuration with $N_a = \log_2(M)$, which gives the best performance; and comparable results in [12] confirm the effectiveness of this conclusion.

Fig. 6 presents both the false alarm probability P_{fa} and the missed detection probability P_{md} for GRSM-4QAM and GRSM-16QAM. In GRSM-16QAM, energy-dependent variations are evident: the higher energy levels $E_2 = 10$ and $E_3 = 18$ exhibit exponential decay in both error components. At low to moderate SNRs, the lowest energy level $E_1 = 2$ in GRSM-16QAM contributes more to errors than the same energy level in GRSM-4QAM. This is due to a smaller non-centrality parameter in GRSM-16QAM, which reduces the separation between received energy distributions and impairs the spatial detector's ability to distinguish between symbols. In contrast, the rapid error decay for E_2 and E_3 significantly improves the overall GRSM-16QAM performance in these SNR ranges. At high SNRs, the error contributions from E_2 and E_3 become negligible due to their large non-centrality parameters under low-noise conditions. As a result, the lowest energy level E_1 dominates overall performance. Since P_{fa} and P_{md} for E_1 are higher in GRSM-16QAM than in GRSM-4QAM, GRSM-16QAM underperforms GRSM-4QAM in this regime, explaining the crossover observed in Fig. 5.

Fig. 7 shows an improved data detection probability P_{em} in GRSM-4QAM in comparison to GRSM-16QAM , in moderate to high SNR regions. That is due to a higher average number of active receiver branches in GRSM-4QAM when $N_a = 6$, resulting in a higher average diversity gain.

Fig. 8 illustrates the performance differences in GRSM-16QAM modulation. When the predefined threshold is selected based on perfect knowledge of the current energy level, the resulting performance serves as a lower bound on the error across all components. In contrast, the practical method exhibits a deviation due to the use of an estimated energy level, leading to increased error probabilities. These errors arise primarily from inaccurate threshold selection based on the estimated rather than actual energy.

V. Conclusion

In this work, GRSM is employed to enhance spectral efficiency while reducing power consumption. However, the use of additional spatial bits through binary antenna activation patterns increases the system's susceptibility to errors. To address this, an optimal predefined threshold is proposed and validated. The theoretical ABEP is derived using these predefined thresholds, capturing the internal energy levels within the MQAM constellation. This is achieved by framing the problem as an energy sensing task based on the received signal's energy. The theoretical ABEP results are validated through link-level simulations, where the predefined thresholds are selected both optimally and practically. The results show an inverted performance trend in GRSM-MQAM, revealing a trade-off between detection accuracy and energy efficiency. Optimizing the number of active antennas (N_a) and considering all-zero activation patterns emerge as key directions for future work.

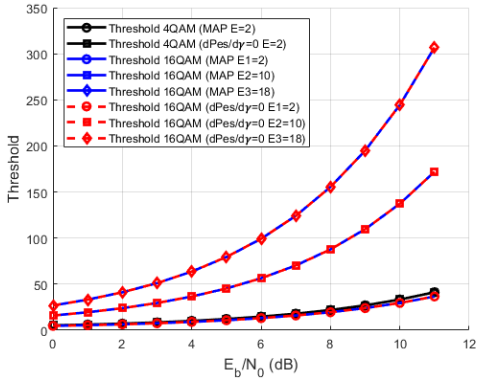

Fig. 4. Threshold validation in GRSM-4QAM, GRSM-16QAM.

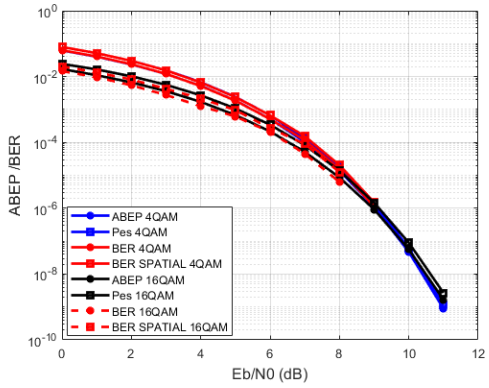

Fig. 5. Comparing both total ABEP, P_{es}, for GRSM-4QAM and GRSM-16QAM, $\alpha_{\text{aver}} = 3.0225$ and $\alpha_{\text{aver}} = 6.6811$, respectively. Results validation using link-level simulations.

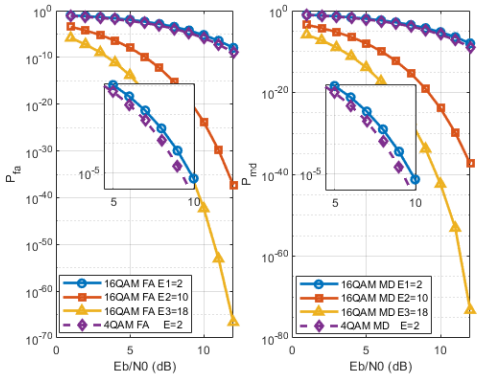

Fig. 6. Comparing both total spatial error components for all energy levels in GRSM-16QAM and GRSM-4QAM.

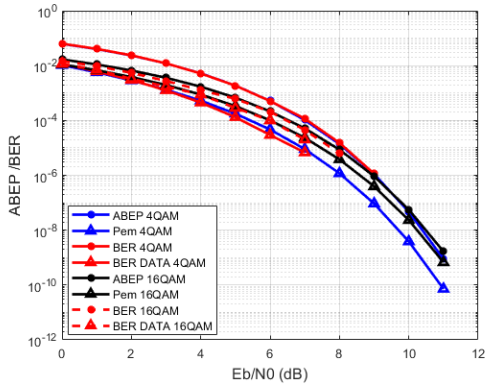

Fig. 7. Comparing both total ABEP, P_{em}, for GRSM-4QAM and GRSM-16QAM, $\alpha_{\text{aver}} = 3.0225$ and $\alpha_{\text{aver}} = 6.6811$, respectively. Results validation using link-level simulations.

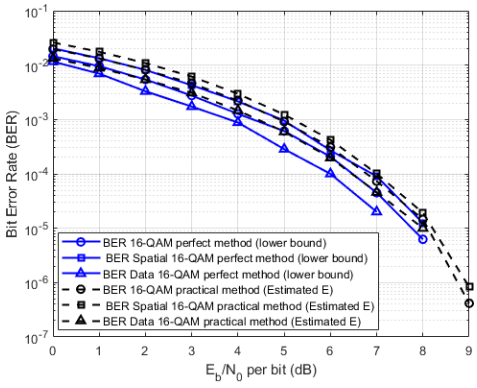

Fig. 8. Comparison of total GRSM-16QAM BER and the spatial and modulation component BER in link-level simulations, considering both the perfect selection and practical selection of the predefined threshold, $\alpha_{\text{aver}} = 6.6811$.

REFERENCES

[1] J. Jeganathan, A. Ghrayeb, and L. Szczecinski, 'Spatial modulation: optimal detection and performance analysis," IEEE Commun. Lett., vol. 12, no. 8, pp. 545–547, Aug. 2008.

[2] R. Zhang, L.-L. Yang, and L. Hanzo, 'Error probability and capacity analysis of generalised precoding aided spatial modulation," IEEE Trans. Wireless Commun., vol. 11, no. 4, pp. 1626–1636, Apr. 2012.

[3] N. S. Perović, P. Liu, M. Di Renzo, and A. Springer, 'Receive spatial modulation for LOS mmWave communications based on TX beamforming," IEEE Trans. Commun., vol. 67, no. 5, pp. 3305–3319, May 2019.

[4] R. Zhang, L.-L. Yang, and L. Hanzo, 'Generalised precoding aided spatial modulation," IEEE Trans. Wireless Commun., vol. 11, no. 3, pp. 1053–1063, Mar. 2012.

[5] A. Raafat, A. Agustin, and J. Vidal, 'Receive spatial modulation for massive MIMO systems," in Proc. IEEE Global Commun. Conf. (GLOBECOM), Singapore, Dec. 2017.

[6] F. B. Mismar and B. L. Evans, 'Variable active antenna spatial modulation," IET Microw., Antennas Propag., vol. 10, no. 15, pp. 1666–1673, Dec. 2016.

[7] M. Saad, F. C. Lteif, A. C. Al Ghouwayel, H. Hijazi, J. Palicot, and F. Bader, 'Generalized spatial modulation in highly correlated channels," in Proc. 2019 IEEE 30th Int. Symp. Personal, Indoor, Mobile Radio Commun. Workshops (PIMRCW), Istanbul, Turkey, 2019, pp. 1–6.

[8] O. El Ayach, S. Rajagopal, S. Abu-Surra, Z. Pi, and R. W. Heath, 'Spatially sparse precoding in millimeter wave MIMO systems," IEEE Trans. Wireless Commun., vol. 13, no. 3, pp. 1499–1513, Mar. 2014.

[9] D. S. Chaves and A. N. Barreto, 'Energy detection spectrum sensing of M-ary QAM systems over AWGN channels," in Proc. 2012 Int. Symp. Wireless Commun. Syst. (ISWCS), Paris, France, Aug. 2012, pp. 106–110.

[10] M. K. Simon, Probability distributions involving Gaussian random variables: A handbook for engineers and scientists. New York, NY, USA: Springer, May 2007.

[11] R. G. Gallager, 'Detection, decisions, and hypothesis testing," in Stochastic Processes: Theory for Applications, Cambridge, U.K.: Cambridge Univ. Press, 2013, pp. 375–416.

[12] N. S. Perović, P. Liu, and A. Springer, 'Bit error probability of preprocessing aided spatial modulation based on MMSE precoding," in Proc. 2015 IEEE 26th Annu. Int. Symp. Personal, Indoor, Mobile Radio Commun. (PIMRC), Hong Kong, Sept. 2015.